^{25}Si and ^{29}S studied via single neutron knockout reactions

R. R. Reynolds,[1] P. D. Cottle,[1] A. Gade,[2,3] D. Bazin,[2,3] C. M. Campbell,[2,3] J. M. Cook,[2,3] T. Glasmacher,[2,3] P. G. Hansen,[2,3] T. Hoagland,[2] K. W. Kemper,[1] W. F. Mueller,[2] B. T. Roeder,[1] J. R. Terry,[2,3] and J. A. Tostevin[4]

[1]*Physics Department, Florida State University, Tallahassee, Florida 32306, USA*

[2]*National Superconducting Cyclotron Laboratory, Michigan State University, East Lansing, Michigan 48824, USA*

[3]*Department of Physics and Astronomy, Michigan State University, East Lansing, Michigan 48824, USA*

[4]*Department of Physics, Faculty of Engineering and Physical Sciences, University of Surrey, Guildford, Surrey GU2 7XH, United Kingdom*

(Received 15 February 2010; published 15 June 2010)

The γ-ray spectroscopy of ^{25}Si and ^{29}S has been performed using single neutron knockout reactions with intermediate energy beams of the exotic isotopes ^{26}Si and ^{30}S. Two γ rays have been observed in ^{25}Si and three in ^{29}S. These are the first γ rays observed in these two isotopes. These two nuclei appear to be well deformed, and possible future intermediate-energy Coulomb excitation measurements would confirm their rotational nature.

DOI: 10.1103/PhysRevC.81.067303 PACS number(s): 25.60.Je, 21.60.Cs, 23.20.Lv, 27.30.+t

While it has long been known that several stable nuclei near the middle of the *sd* shell are well-deformed (for example, see Refs. [1–3]), the advent of high-quality beams of exotic nuclei in this mass region has provided a new opportunity to map the presence of deformation in the nearby proton-rich isotopes (for example, see Refs. [4–6]). In the present work, we report on a spectroscopic study of the isotopes ^{25}Si and ^{29}S using the intermediate energy single neutron knockout reaction that yields the first observations of γ rays in these isotopes and provides evidence that the region of deformation in the mid-*sd* shell extends to these $T_z = -3/2$ nuclei. The present reaction selectively populates states that have the structure of a neutron hole coupled to the projectile nuclei. In fact, the most strongly populated states in the present study were the ground states in ^{25}Si and ^{29}S because they correspond to the coupling of $d_{5/2}$ neutron holes to the parent nuclei. However, admixtures of small fragments of strength from all the *sd* neutron orbits—$s_{1/2}$, $d_{3/2}$, and $d_{5/2}$—into the rotational states allowed the observation of such states having $J^\pi = 1/2^+$, $3/2^+$, and $5/2^+$. The data compiled in the review of Sorlin and Porquet [7] indicates that the gap between the single neutron energy of the $d_{5/2}$ orbit and the energies of the $s_{1/2}$ and $d_{3/2}$ orbits is at least 5 MeV. Therefore, the main concentrations of $s_{1/2}$ and $d_{3/2}$ neutron hole strength cannot be observed in the present study because they occur above the proton separation energies, which are 3.4 MeV in ^{25}Si and 3.3 MeV in ^{29}S. Shell model calculations suggest that the states seen here are connected by strong $E2$ transitions characteristic of well-deformed nuclei. The addition of data from intermediate-energy Coulomb excitation measurements would quantify the extent of deformation in these isotopes.

A primary beam of 150 MeV/nucleon ^{36}Ar was produced by the Coupled Cyclotron Facility at the National Superconducting Cyclotron Laboratory. The primary beam impinged on a ^{9}Be production target at the midacceptance position of the A1900 fragment separator [8]. The secondary beams of ^{26}Si and ^{30}S were then steered onto a 376 mg/cm^2 ^{9}Be secondary target located at the pivot point of the S800 large acceptance magnetic spectrograph [9]. The secondary target was surrounded by SeGA [10], an array of 17 high-purity 32-fold segmented germanium detectors.

The incident secondary beam was composed of a cocktail of nuclear species. ^{26}Si comprised 13% of the cocktail beam and had a midtarget velocity of 0.446c, which corresponds to a midtarget energy of 109 MeV/nucleon. ^{30}S comprised 11% of the beam and had a midtarget velocity of 0.435c, giving a midtarget energy of 103 MeV/nucleon. Projectilelike residues from reactions with the secondary target were identified using time-of-flight information and the S800's focal plane detectors [11].

The segmentation of SeGA allowed for an accurate Doppler reconstruction of the emitted γ rays into the rest frame of the emitting nucleus at the time of emission (assumed to be midtarget). GEANT [12] was used to determine the γ ray yields taking into account the changes in the Doppler energy shifts at the different angles of emission/detection and the energy dependence of the detection efficiency. The γ-ray spectra of ^{25}Si and ^{29}S, along with the GEANT fits to the spectra, are shown in Fig. 1.

The inclusive cross sections for the ^{9}Be(^{26}Si,^{25}Si)X and ^{9}Be(^{30}S,^{29}S)X reactions were calculated from the ratio of detected residues in the S800 focal plane to the number of incoming secondary beam particles per number density of the ^{9}Be target. There were a few sources of systematic uncertainty that arise in the inclusive cross-section measurements: the uncertainty of the particle identification software gates ($\sim$5%), uncertainties arising from fluctuations in the beam purity and stability ($<$5%), and the corrections for the limited momentum/angle acceptance of the S800 ($<$10%). These uncertainties were taken into consideration and added in quadrature to the statistical errors.

The cross sections for individual excited states in the final residues were determined using the ratios of particle-γ coincidence events to the total population of the inclusive residue reaction channel. The GEANT simulations were used to make efficiency corrections to the number of observed γ rays to determine the total number of γ-ray emissions. The simulations were normalized to agree with stationary source

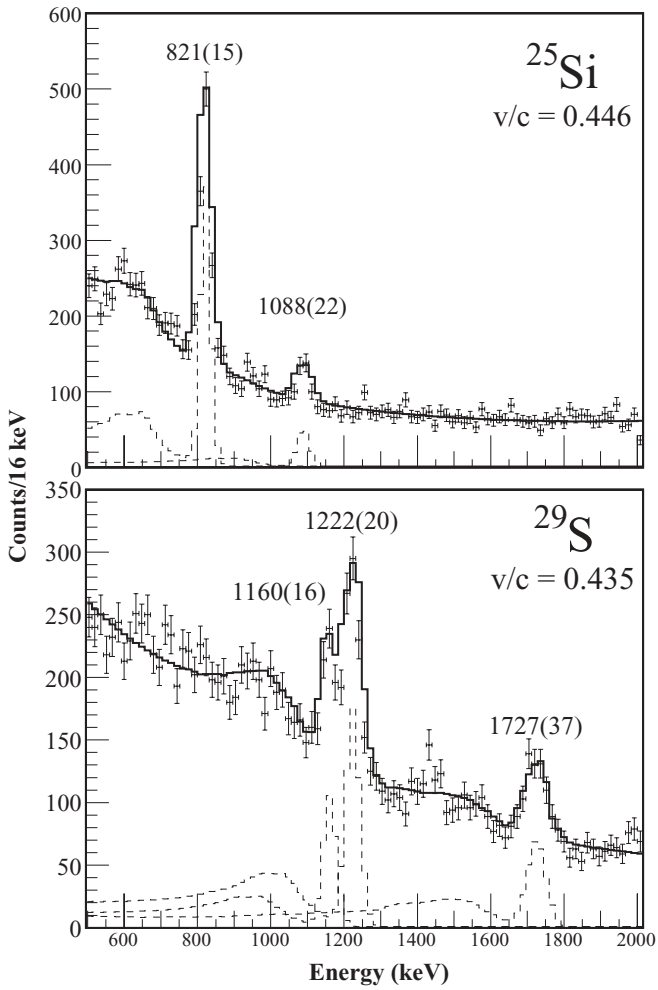

FIG. 1. Doppler-reconstructed γ-ray spectra. The γ-ray energies are reconstructed into the rest frame of the projectile of interest at the midtarget velocity (v/c). The dashed lines are the GEANT [12] simulated photo peaks and the solid lines are the summed simulated photo peaks added to a smooth fitted background function.

runs made during the experiment. The ground-state cross sections were determined by subtracting the contributions of the observed excited states from the inclusive cross sections. The results can be seen in Table I. The statistics were not sufficient to support any particle-γ-γ coincidence measurements.

Single neutron knockout reaction model calculations were made using the sudden and eikonal approximations [16]. The theoretical cross section for populating a specific nuclear state with spin-parity J^π is

$$\sigma_{\rm th}(J^\pi) = \left(\frac{A}{A-1}\right)^N C^2S\sigma_{\rm sp}(J, l, S_n + E_x). \qquad (1)$$

Here A is the mass of the projectile, N is the main oscillator number (for the *sd* shell, $N = 2$), C^2S is the spectroscopic factor taken from shell model calculations, and the effective neutron separation energy $S_n + E_x$ is the sum of the neutron separation energy from the projectile ground state plus the excitation energy of the final state of the residue nucleus. $\sigma_{\rm sp}$ is the theoretical single particle cross section calculated by adding together the contributions from the nucleon stripping mechanism and diffractive dissociation with all parameters constrained according to the procedure outlined in Ref. [17].

In both knockout reactions discussed here, the projectile and residual nuclei can be described in the *sd*-shell model space. For the purposes of this study we used the USDB Hamiltonian [14] to calculate the theoretical spectroscopic factors ($C^2S_{\rm SM}$) and excited-state energies. The shell-model calculations were performed using CoSMo [13].

The level scheme for ^{25}Si, as seen in Fig. 2, was determined by comparing the observed γ-ray energies to the energy levels observed in Ref. [15] and the shell-model calculations. The low-lying 40-keV state seen in Ref. [15] is below the low energy limit for detection of γ rays by SeGA, so the direct population of this level cannot be separated from the ground-state cross-section measurement. The observed excited-state energies are in good agreement with the previously observed energies. The possibility of the 1089- and 821-keV γ rays decaying from the same state was ruled out because there was no observable state at 268 keV to corroborate this scenario. The 821-keV γ ray is assumed to decay directly to the ground state because of the observed 815-keV level reported in Ref. [15]. The observed 1088-keV decay corresponds to a decay from the 1909-keV level to the 821-keV level. There was no observable decay from the 1909-keV state to the ground state or the 40-keV state. Considering the efficiency of detecting a γ ray of energy near 1900 keV, it would be detectable if it had an efficiency-adjusted intensity about equal to that of the 1088-keV γ ray. The states observed in the mirror reaction, ^{26}Mg(d,^{3}He)^{25}Na [18] are also shown in Fig. 2. The similarities in the mirror nuclei lend confidence to our conclusions.

The level scheme for ^{29}S is shown in Fig. 3. The level assignments and decay schemes were determined by comparisons of the observed γ-ray energies to the shell-model calculations. The $7/2^+$ level at 1727 keV should not be directly populated in this reaction, but is instead fed indirectly from the 2887-keV level via the 1160-keV γ ray. This is corroborated by the similar γ-ray intensities observed for the 1160- and 1727-keV γ rays. The 2887-keV level is assigned to the lowest excited $5/2^+$ state based on the dominant $C^2S_{\rm SM}$ value calculated. The direct decay of the 2887-keV level to the ground state was not observed, but given the efficiency of measuring a 2887-keV γ ray, the intensity has to be less than half of the intensity of the observed 1160-keV decay branch. The 1222-keV γ ray is assumed to correspond to the first excited state at $1/2^+$. Figure 3 also includes states seen in the mirror system, observed in the reaction ^{30}Si(t,α)^{29}Al [19]. Once again, the similarities in the results of the mirror nuclei support the present conclusions.

Extensive measurements have now demonstrated that cross sections measured in $(e, e'p)$ and single-nucleon knockout reactions are systematically lower than theoretical predictions based on single particle strengths deduced from shell-model calculations [17]. Reductions in the cross sections, interpreted as reductions in the effective spectroscopic strengths, can be

TABLE I. The deduced level energies E_{level}, associated γ-ray decay energies E_γ, measured cross sections σ_{exp}, theoretical single particle reaction cross sections σ_{sp} and the theoretical cross sections σ_{th} from Eq. (1), C^2S values obtained from the USDB shell model calculations, and reduction factors R_s.

Residue	E_{level} (keV)	E_γ (keV)	σ_{exp} (mb)	J^π [a]	σ_{sp} (mb)	C^2S_{SM} [b]	σ_{th} (mb)	R_s [c]
^{25}Si	1909(27)	1088(22)	1.06(21)	$(3/2^+)$	12.10	0.18	2.36	
	821(15)	821(15)	4.06(61)	$(1/2^+)$	13.44	0.25	3.64	
	40(5)[d]			$(3/2^+)$	12.68	0.12	1.65	
	G.S.			$(5/2^+)$	13.53	2.73	40.0	
	G.S. + 40 keV		21.0(35)				41.6	0.50(9)
	Inclusive		26.1(35)				47.6	0.55(7)
^{29}S	2887(40)	1160(16)	1.86(15)	$(5/2^+)$	10.89	0.80	9.32	
	1727(37)	1727(37)		$(7/2^+)$				
	1222(20)	1222(20)	3.09(33)	$(1/2^+)$	12.68	0.36	4.89	
	G.S.		22.6(27)	$(5/2^+)$	11.80	3.63	45.9	0.49(6)
	Inclusive		27.5(26)				60.1	0.46(4)

[a]Tentatively assigned from comparison with shell-model calculations.
[b]Calculated with CoSMo [13] and the USDB effective interaction [14].
[c]Defined as described in the text.
[d]Taken from Ref. [15].

stated as a reduction factor defined as

$$R_S = \frac{\sigma_{\text{exp}}}{\sigma_{\text{th}}}. \tag{2}$$

The reduction factor thus represents the ratio of the observed spectroscopic strength to that of the shell model calculations. It can be studied as a function of the asymmetry ΔS between the neutron and proton separation energies (S_n and S_p). For the case of neutron removal, $\Delta S = S_n - S_p$ [17]. Thus, a large negative ΔS corresponds to the removal of a weakly bound neutron while a large positive value corresponds to the removal of a strongly bound neutron. The reduction factors have recently been catalogued for a wide range of ΔS values [17]. It has been observed that the spectroscopic strength for the removal of weakly bound nucleons is close to the values predicted in the single particle models. In contrast, the removal of a strongly bound nucleon results in a more appreciable reduction of the spectroscopic strength. As more data are collected from exotic species of nuclei, the relationship

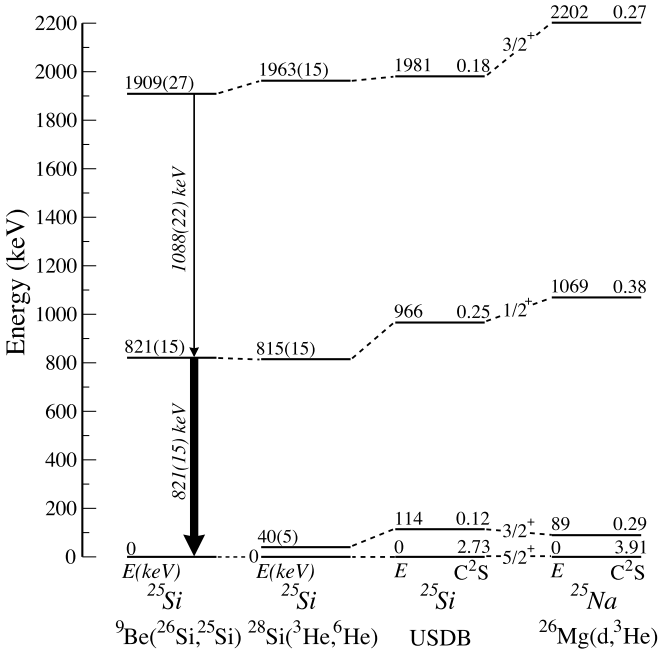

FIG. 2. (Level schemes from left to right) ^{25}Si determined from the current work, ^{25}Si from Ref. [15], ^{25}Si from the USDB shell model, and from the isospin mirror ^{25}Na from Ref. [18]. The J^π values shown correspond to those given by the shell-model calculations.

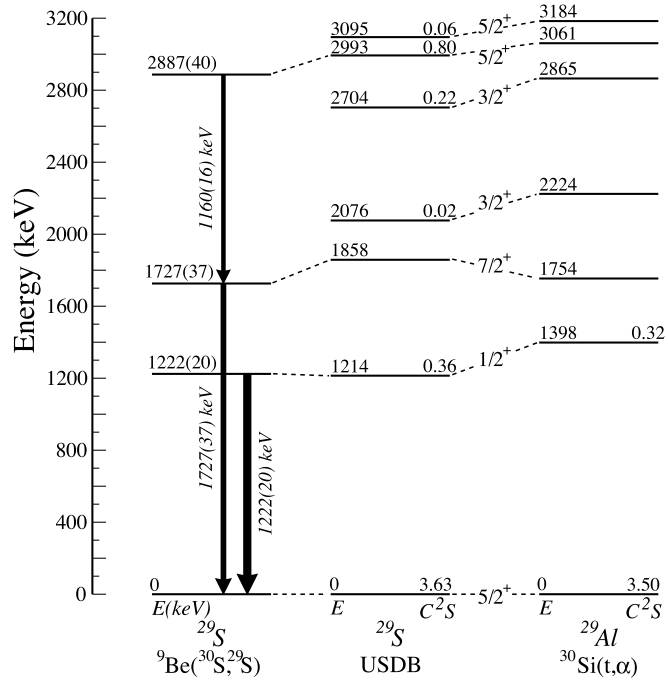

FIG. 3. (Level schemes from left to right) ^{29}S determined from the current work, ^{29}S from the USDB shell model, and from the isospin mirror ^{29}Al from Ref. [19]. The J^π values shown correspond to those given by the shell-model calculations.

between the reduction factors and ΔS is becoming more evident (see Fig. 6 in Ref. [17]).

For ^{26}Si, the S_n and S_p energies are 19041(10) and 5518(3) keV, respectively, leading to $\Delta S = 13.5$ MeV. Observing the results recorded in Fig. 6 of Ref. [17], we would expect the reduction factor $R_S \approx 0.4$, and our observed inclusive R_S was 0.55(7). In ^{30}S, $S_n = 18980(50)$ keV and $S_p = 4400(3)$ keV, so the expected R_S for $\Delta S = 14.6$ MeV, is also around 0.4, while the observed inclusive value was 0.46(4). Reduction factors for states with small spectroscopic factors would be expected to vary considerably because of the difficulty of calculating small spectroscopic factors reliably. Therefore, the only reduction factors included in the table are those for the ground state and inclusive cross sections.

While the large cross sections observed here and the shell-model calculations suggest that the ground states of ^{25}Si and ^{29}S have strong $d_{5/2}$ neutron hole components, the remaining states seen here appear to be predominantly rotational in nature. The 821- and 1909-keV states in ^{25}Si and the 1222- and 2887-keV states in ^{29}S have small neutron-hole components and are therefore weakly populated in the neutron knockout reaction. The 1727-keV state in ^{29}S does not appear to be directly populated, but is observed here because the 2887-keV state decays to it via the 1160-keV transition.

The shell-model calculations provide predictions of the strengths of the $E2$ transitions connecting the states observed here. In ^{25}Si, the calculation with the USDB effective interaction gives a strongly collective 15-Weisskopf-unit (W.u.) $E2$ connecting the ground state and the $1/2^+$ state that is calculated to be at 966 keV and which is observed here to be at 821 keV. The 1088-keV transition connecting the state observed at 1909 keV (corresponding to a $3/2^+$ state calculated to be at 1981 keV) with the 821-keV state is—according to the calculation—dominated by the $M1$ multipolarity, although a strong 9-W.u. $E2$ component is involved as well.

In ^{29}S, the observed 1222-keV state appears to correspond to a $1/2^+$ state calculated to occur at 1214 keV. The $E2$ transition connecting this state to the ground state is calculated to have a strength of 6.2 W.u., which is significantly less collective than is typical for rotational bands in this region. However, the shell-model calculation gives a collective $E2$ transition between the ground state and the 1858-keV $7/2^+$ with a strength of 16 W.u. This $7/2^+$ state from the shell-model calculation probably corresponds to the observed 1727-keV state.

The ^{29}S state observed at 2887 keV probably corresponds to a $5/2^+$ state calculated to occur at 2993 keV. The dominant decay of this state is calculated to be to the 1858-keV state (corresponding to the observed 1727 keV) via an $M1$ transition, as seen in the experiment.

In each of the two nuclei measured here, we have observed one state that the shell-model calculation indicates should be connected to the ground state by a strong $E2$ transition. These states, at 821 keV in ^{25}Si and 1727 keV in ^{29}S, can be interpreted as rotational excitations of the ground state. Of course, the present experiment does not confirm these rotational interpretations. Intermediate Coulomb excitation measurements [20] of these two isotopes would provide direct measurements of the strengths of these two $E2$ transitions and confirm and quantify their rotational natures.

This work was supported by the National Science Foundation under Grant Nos. PHY-0606007, PHY-0355129, and PHY-0653323. A.G. is supported by the Alfred P. Sloan Foundation. J.A.T. is supported by the United Kingdom Science and Technology Facilities Council (STFC) through Research Grant No. ST/F012012.

[1] A. E. Litherland, E. B. Paul, G. A. Bartholomew, and H. E. Gove, Phys. Rev. **102**, 208 (1956).
[2] D. A. Bromley, H. E. Gove, and A. E. Litherland, Can. J. Phys. **35**, 1057 (1957).
[3] A. E. Litherland, H. McManus, E. B. Paul, D. A. Bromley, and H. E. Gove, Can. J. Phys. **36**, 378 (1958).
[4] P. D. Cottle *et al.*, Phys. Rev. Lett. **88**, 172502 (2002).
[5] E. Khan *et al.*, Nucl. Phys. A **694**, 103 (2001).
[6] P. D. Cottle, B. V. Pritychenko, J. A. Church, M. Fauerbach, T. Glasmacher, R. W. Ibbotson, K. W. Kemper, H. Scheit, and M. Steiner, Phys. Rev. C **64**, 057304 (2001).
[7] O. Sorlin and M.-G. Porquet, Prog. Part. Nucl. Phys. **61**, 602 (2008).
[8] D. J. Morrissey *et al.*, Nucl. Instrum. Methods Phys. Res. B **204**, 90 (2003).
[9] D. Bazin *et al.*, Nucl. Instrum. Methods Phys. Res. B **204**, 629 (2003).
[10] W. F. Mueller *et al.*, Nucl. Instrum. Methods Phys. Res. A **466**, 492 (2001).
[11] J. Yurkon, D. Bazin, W. Benenson, D. J. Morrissey, B. M. Sherrill, D. Swan, and R. Swanson, Nucl. Instrum. Methods Phys. Res. A **422**, 291 (1999).
[12] CERN Program Library Long Writeup W5013 (1993).
[13] D. Morris and A. Volya, [http://cosmo.volya.net] (2009).
[14] B. A. Brown and W. A. Richter, Phys. Rev. C **74**, 034315 (2006).
[15] W. Benenson, J. Driesbach, I. D. Proctor, G. F. Trentelman, and B. M. Preedom, Phys. Rev. C **5**, 1426 (1972).
[16] P. G. Hansen and J. A. Tostevin, Annu. Rev. Nucl. Part. Sci. **53**, 219 (2003).
[17] A. Gade *et al.*, Phys. Rev. C **77**, 044306 (2008).
[18] R. Firestone, Nucl. Data Sheets **110**, 1691 (2009).
[19] J. S. Hanspal, K. I. Pearce, N. M. Clarke, R. J. Griffiths, R. E. Brown, R. A. Hardekopf, and W. Gruebler, Nucl. Phys. A **455**, 494 (1986).
[20] J. M. Cook, T. Glasmacher, and A. Gade, Phys. Rev. C **73**, 024315 (2006).